JTTEE5 6:91-98

Thermal Barrier Coating Life Modeling in Aircraft Gas Turbine Engines

D.M. Nissley

Analytical models for predicting ceramic thermal barrier coating (TBC) spalling life in aircraft gas turbine engines are presented. Electron beam/physical vapor-deposited and plasma-sprayed TBC systems are discussed. An overview of the following TBC spalling mechanisms is presented: (1) metal oxidation at the ceramic/metal interface, (2) ceramic/metal interface stresses caused by radius of curvature and interface roughness, (3) material properties and mechanical behavior, (4) component design features, (5) temperature gradients, (6) ceramic/metal interface stress singularities at edges and corners, and (7) object impact damage. Analytical models for TBC spalling life are proposed based on observations of TBC spalling and plausible failure theories. Spalling was assumed to occur when the imposed stresses exceed the material strength (at or near the ceramic/metal interface). Knowledge gaps caused by lack of experimental evidence and analytical understanding of TBC failure are noted. The analytical models are considered initial engineering approaches that capture observed TBC spalling failure trends.

Keywords analytical models, spalling mechanisms, thermal barrier coatings

1. Introduction

SINCE the 1950s the rotor inlet temperature of aircraft gas turbines has risen at a rate of about 22 °C (40 °F) per year (Ref 1). This rise in operating temperature has been accommodated by improved cooling methods and superalloys such as nickel-base single crystals. However, as cost-effective cooling and superalloy advancements become exhausted, TBC insulation is required to shield the turbine superalloy components from the increasingly severe temperature environment.

Thermal barrier coatings (TBCs) are a powerful cooling method. Each 0.025 mm (0.001 in.) of TBC thickness provides up to 17 to 33 °C (30 to 60 °F) temperature reduction, depending on the TBC ceramic structure and level of convective cooling (Ref 2). However, TBC delamination and spalling in hot-section components may occur before reaching the component design life requirement. Local TBC spalling introduces a hot-spot condition in the substrate, which aggravates substrate oxidation and thermomechanical fatigue (TMF) crack initiation (e.g., Ref 3). As a result, the full TBC cooling benefit cannot be realized. Cooling air is needed to counteract the effect of hot regions caused by local TBC failure. Accurate TBC life prediction models are needed to optimize cooling flows, reduce component design and development costs, and create avenues for TBC material and/or processing improvements.

Thermal barrier coating systems used in aircraft gas turbines are fabricated by plasma spray or electron beam/physical vapor deposition (EB-PVD). These TBC systems nominally consist of a 0.127 mm (0.005 in.) MCrAlY bond coat and a 0.254 mm (0.010 in.) ceramic top coat. The bond coat is needed to prevent oxidation of the substrate material and provide good bonding of the ceramic. Yttria partially stabilized zirconia (nominally 7 wt% Y) is typically used for the ceramic top coat. The typical structure of plasma-sprayed and EB-PVD TBC coatings is shown in Fig. 1. Plasma-sprayed TBC is a bulk coating in which the as-deposited ceramic contains microdefects. Plasma-sprayed TBC failure occurs just above the metallic bond coating in the ceramic material. Ceramic delamination cracks initiate very near (or at) peaks in the rough bond coating and propagate along the interface in the ceramic layer. An EB-PVD ceramic has a columnar structure as a result of the vapor deposition process. Failure in an EB-PVD TBC occurs in the thermally grown oxide (TGO) layer adjacent to the metallic bond coating. Most

D.M. Nissley, Pratt & Whitney, a United Technologies Company, 400 Main Street, East Hartford, CT 06108, USA.

Symbols

N_f	TBC spalling life in cycles
Q/A	heat flux
R	wavy interface amplitude
t	ceramic coating thickness
y	distance along the ceramic/metal interface
E_c, ν_c	ceramic elastic modulus and Poisson's ratio
E_s, ν_s	substrate elastic modulus and Poisson's ratio
α_c, k_c	ceramic thermal expansion coefficient and thermal conductivity
δ	metal oxide thickness
δ_c	metal oxide thickness that causes TBC spalling in one cycle
$\Delta\alpha\Delta T$	ceramic/metal thermal expansion mismatch strain
$\Delta\varepsilon_f$	effective TBC spalling inelastic strain range
$\Delta\varepsilon_{fo}$	ceramic inelastic strain range that causes TBC spalling in one cycle in the absence of oxidation
$\Delta\varepsilon_{in}$	ceramic inelastic strain range
λ	wavy interface wavelength
ρ	local radius of curvature
σ_n	stress perpendicular to the ceramic/metal interface
σ_θ	ceramic stress parallel to the ceramic/metal interface

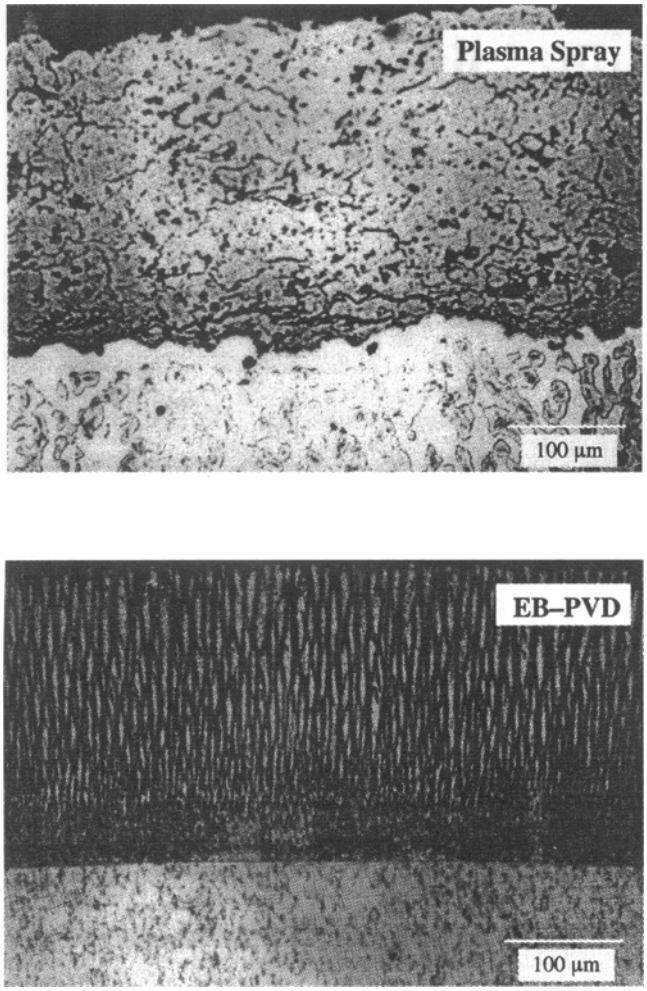

Fig. 1 Typical microstructures of TBC coatings

of the TGO in EB-PVD TBC remains adherent to and is lost with the ceramic during a spall event.

Crack initiation and growth to a critical size in TBCs is predominantly associated with the stress field at TBC microdefect locations. Microdefects can be produced by the fabrication process or by high-temperature thermal exposure. Both in-plane (parallel to the ceramic/metal interface) and out-of-plane (perpendicular to the ceramic/metal interface) stresses can be present. For example, the typical bulk residual stress state in the nonmetal layer adjacent to the interface around the circumference of a tube combines in-plane compression and out-of-plane tension. The bulk stresses interact with the microdefect structure to promote crack initiation and growth. Then, when the near-interface crack(s) has grown to a critical size, the TBC fails by spalling. Spalling (far from edges and corners) is usually caused by coating buckling (Ref 4, 5).

Initial engineering TBC spalling life correlations were accomplished by charting the observed TBC life versus temperature. Thermally grown oxide formation was considered the primary TBC delamination cracking mechanism. Temperature was used as an indirect measurement of TGO formation at the ceramic/metal interface. By the end of the 1980s, more sophisticated TBC spalling life prediction models were developed (Ref 6-8). These improved models captured TBC spalling life by combining a structural analysis of the TBC (i.e., substrate, bond coat, and ceramic) with the accumulated TGO thickness. However, further investigation of TBC spalling mechanisms and modifications to TBC life models are needed to adequately capture TBC spalling life. Areas of investigation and model modifications are suggested herein.

2. Overview of TBC Spalling Mechanisms

2.1 *Metal Oxidation (TGO Formation)*

Thermally grown oxide formation due to metal bond coat oxidation is a volumetric expansion process that occurs during high-temperature exposure. The volume change is constrained in the plane of the interface because the stiffness of the TGO is insignificant relative to the stiffness of the substrate. As a result, the TGO forms with a residual compressive stress. Upon cooling to ambient conditions, the TGO is forced further into compression. It is speculated that TGO formation creates (or increases) the normal stress perpendicular to the ceramic/metal interface at microdefect sites in either the (plasma-sprayed TBC) ceramic or (EB-PVD TBC) TGO layer. However, based on static furnace tests, it is known that TGO formation by itself is insufficient to cause TBC spalling. No TBC failures were observed in static furnace oxidation tests so long as the specimens remained in the furnace. The TBC spalled when the specimens were removed from the furnace and cooled to ambient conditions (Ref 6-8).

2.2 *Radius of Curvature*

The local radius of curvature directly affects the stress perpendicular to the interface, σ_n (Ref 4, 5). Consistent with the observation that TBC spalling is a buckling phenomenon, the ceramic stress parallel to the interface, σ_θ, is compressive. Then on concave surfaces, such as on the pressure surface of airfoils, σ_n is compressive, and on convex surfaces, such as airfoil suction surfaces, σ_n is tensile. In general, a finite-element analysis is used to determine σ_n, but isothermal conditions can be modeled by using a thin-wall pressure vessel formula:

$$\sigma_n = \rho t \sigma_\theta \qquad \text{(Eq 1)}$$

where ρ is the local radius of curvature and t is the coating thickness.

2.3 *Interface Roughness*

Interface roughness (or waviness) is considered a stress concentration that affects the local level of σ_n. For plasma-sprayed TBC, a residual σ_n develops that is tensile at the bond coat peaks and compressive at the bond coat valleys (Ref 4). The ceramic/metal interface of an EB-PVD TBC is smooth relative to a plasma-sprayed TBC. Thus, the contribution of interface roughness to the residual σ_n in an EB-PVD coating is considered small. As an initial approach, Evans et al. (Ref 4) proposed the solution of an isolated cylindrical inclusion:

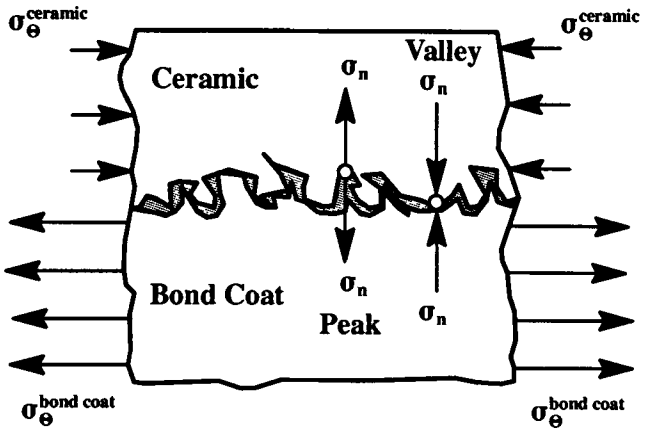

Fig. 2 Interface roughness effect on the local residual stress field. Source: Based on Ref 4

Table 1 Effects of sintering on sprayed zirconia properties

Sintering condition	Room-temperature normalized properties(a) $\frac{\sigma_f}{\sigma_{fo}}$	$\frac{E}{E_o}$	$\frac{k}{k_o}$	$\frac{\varepsilon_f}{\varepsilon_{fo}}$
As sprayed	1.00	1.00	1.00	1.00
5 h at 1093 °C (2000 °F)	1.19	1.12	...	...
36 h at 1093 °C (2000 °F)	1.42	1.32	...	...
24 h at 1288 °C (2350 °F)	2.80	4.70	...	0.25
1 h at 1427 °C (2600 °F)	3.50	3.10	...	...
5 h at 1593 °C (2900 °F)	3.61	4.10	...	0.20
36 h at 1593 °C (2900 °F)	3.68	4.17	2.53	0.20

(a) σ_f, failure strength; E, elastic modulus; k, thermal conductivity; ε_f, failure strain; σ_{fo}, E_o, k_o, and ε_{fo}, as-sprayed properties

$$\sigma_n \approx \frac{[\Delta\alpha\Delta T][1/\kappa + E_c(1+\nu_c)(R\rho)]\sin(2\pi y/\lambda)}{1+R/t} \quad \text{(Eq 2)}$$

$$\kappa = \frac{(1+\nu_c)}{2E_c} + \frac{(1-2\nu_s)}{E_s} \quad \text{(Eq 3)}$$

The interface roughness effect is presented in Fig. 2. Equation 2 generates stress trends in qualitative agreement with the finite-element results of Chang et al. (Ref 9).

2.4 *Ceramic Sintering*

As-deposited ceramics can sinter rapidly when exposed to temperatures above 1093 °C (2000 °F). The sintering process causes significant volumetric and material property changes. Sintering shrinks the ceramic and introduces in-plane tensile stress that can cause cracks perpendicular to the interface (i.e., mudflat cracks). Typically, the ceramic becomes stiffer and more linearly elastic with a commensurate decrease in ductility. Thermal conductivity generally increases. The effects of sintering on a plasma-sprayed zirconia ceramic are presented in Table 1. In EB-PVD coatings, the columnar structure can be destroyed by sintering. The long-term effect of ceramic sintering on TBC spalling needs further experimental and analytical investigation.

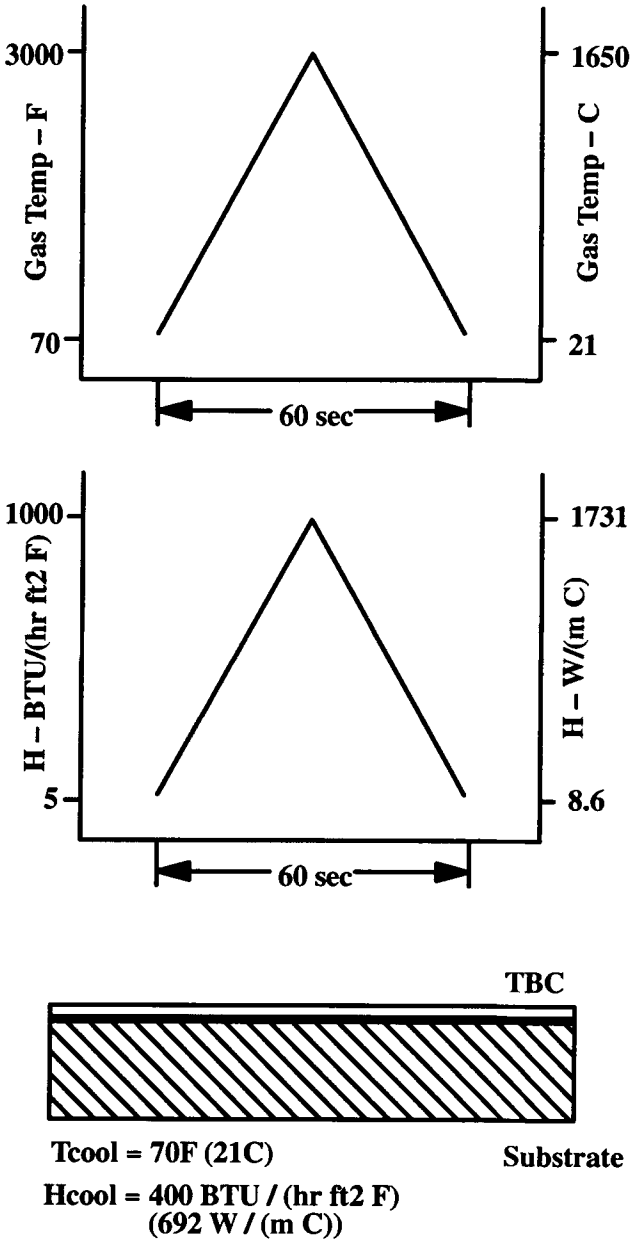

Fig. 3 Boundary conditions used for heat-transfer and structural analysis of TBC

2.5 *Material Constitutive Behavior*

2.5.1 Ceramics

Ceramics are often considered elastic materials; however, it is known that TBC ceramics can also behave in an apparent inelastic fashion (Ref 6-8). Tensile inelastic deformation and stress relaxation can increase the residual in-plane compressive stress that contributes to TBC spalling.

Unified viscoplastic models can be modified to capture the first-order apparent inelastic behavior of TBC ceramics (Ref 6-8). As an example, a transient heat transfer and nonlinear structural analysis was performed on a TBC-coated flat plate using an enhanced version of the LAYER finite-element program (Ref 10). Substrate and TBC heat-transfer boundary conditions are presented in Fig. 3. The substrate was 2.29 mm (0.090 in.) MAR-M509 with a 0.127 mm (0.005 in.) MCrAlY bond coat and a 0.254 mm (0.010 in.) ceramic top coat. The analysis proceeded until three consecutive thermal cycles were completed. Structural analysis results are presented in Fig. 4 and 5 for the third cycle of the analysis. In turbine applications, plasma-sprayed ceramics exhibit cyclic inelasticity; however, EB-PVD ceramics are virtually elastic in the normal turbine operating temperature range. The EB-PVD columnar structure, unlike a plasma-sprayed ceramic, is considered incapable of withstanding significant tensile stress (Ref 7, 8). The EB-PVD constitutive model captures tensile straining by assuming that the ceramic columns break apart when subjected to tensile stress. Then, upon reverse loading, the ceramic columns are brought together before compressive stress is imposed.

2.5.2 TGO

The TGO is very thin (less than about 13 μm, or 5×10^{-4} in.). Because of its thinness and because it exists underneath the ceramic layer, TGO constitutive behavior has not yet been determined experimentally. Thermally grown oxide behavior is typically assumed to be elastic with material properties equal to Al_2O_3 (Ref 7, 8).

2.5.3 Bond Coat

The bond coat is an oxidation-resistant metallic coating, usually of the MCrAlY family, that is plasma sprayed onto the substrate. Such coatings are highly viscoplastic above about 650 °C (1200 °F) and very strong below about 427 °C (800 °F) (Ref 11). As a result, substantial inelastic deformation occurs in the bond coating during thermal cycling. Bond coat nonlinear structural analysis results are shown in Fig. 4 and 5. Chang et al. (Ref 9) suggest that the effect of bond coat inelasticity is small; however, further investigation across the turbine operating temperature range is needed. Considering the effect of interface roughness, it is speculated that bond coats that generate low residual tensile stress upon cooling to room temperature are desirable for improved plasma-sprayed TBC durability.

2.5.4 Substrate

Understanding the inelastic behavior of the substrate is important because the substrate controls the deflections imposed on the TBC (assuming insignificant TBC stiffness). For example, hot-spot component locations can stress-relax quickly and influence the local strain field of the TBC. Many viscoplastic models are currently available for predicting substrate inelastic deformation (e.g., Ref 11-13).

2.6 *Local Component Geometric Design Details*

Normally, no shear stress exists at a smooth ceramic/metal interface unless an interface crack is present (Ref 4). However, some component design details introduce shear stress into the interface by imparting a "punch" load. This situation is similar to an end-supported beam that is loaded at its middle (i.e., three-point bending). Such loading can introduce significant (i.e., >10% of fracture strength) transverse shear stress at the interface. Usually, transverse shear stress occurs at local features such as airfoil pedestal trailing edges and combustor liner welded lap joints.

2.7 *Thermal Gradients*

The maximum in-plane stress usually occurs during transient operating conditions. Whereas the outer ceramic layer responds rapidly to transient thermal conditions, the substrate does not because of the ceramic insulation. The substrate constrains the TBC until enough heat is conducted through the ceramic such that the substrate thermal expansion overtakes the ceramic thermal expansion. For steady-state constant heat flux conditions, Andersson (Ref 5) estimates σ_n for cylindrical geometries by combining Eq 1 with the following formula for stress:

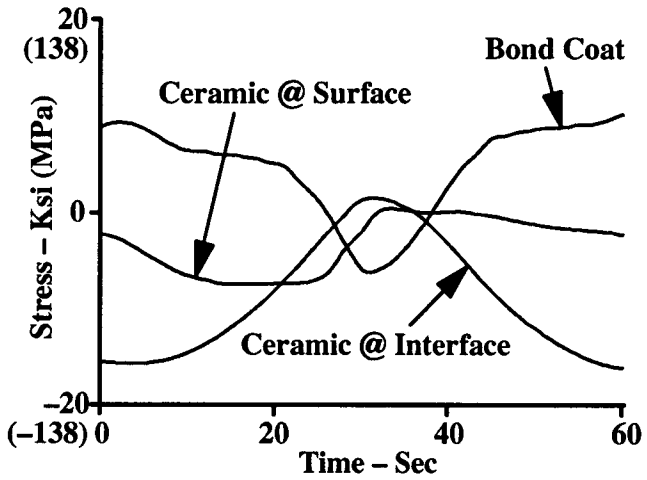

Fig. 4 Constitutive behavior of a plasma-sprayed TBC

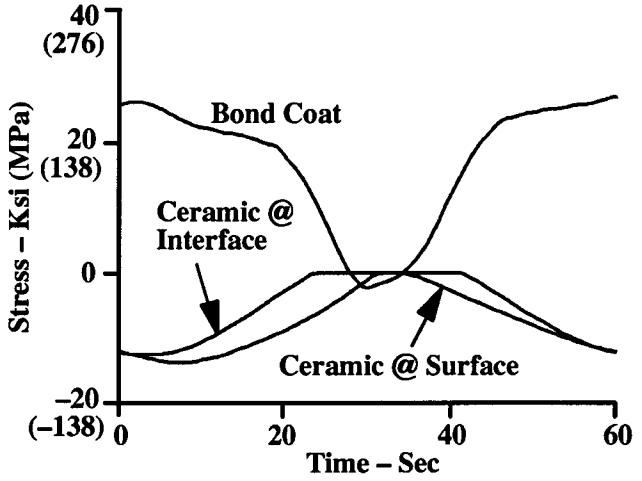

Fig. 5 Constitutive behavior of an EB-PVD TBC

$$\sigma_\theta = -\frac{\alpha_c E_c}{(1-\nu_c)}\frac{Qt}{Ak_c} \qquad \text{(Eq 4)}$$

For a given TBC system, Eq 4 infers that spalling life is reduced as heat flux and ceramic thickness are increased. This is consistent with TBC spalling observations (Ref 6).

2.8 *Stress Singularities at Edges and Corners*

Frequently, TBC spalls originate at component edges or corners such as drilled film cooling holes, airfoil platforms, or blade-tip shrouds. Stress singularities exist at such locations because of dissimilar material properties. As shown in Fig. 6, the edge condition cannot be solved by conventional finite-element analysis because asymmetrical shear violates the theory of elasticity in the element along the edge. As a result, stress singularities are introduced near the edge to satisfy the edge boundary conditions (e.g., Ref 14, 15). Recent numerical modeling trends indicate that stress intensity can be used to model the edge condition. One such approach (Ref 15) involves a hybrid technique that combines the results of finite-element and surface integral analyses to calculate the mode I and mode II stress intensities along the interface. Typical edge stress singularity results are presented in Fig. 7. The relationship between the edge stress intensities and TBC spalling life must be determined experimentally.

2.9 *Impact Damage*

Spalling of TBCs due to object damage can occur when material particles impinge on the ceramic layer (Ref 3). Impact damage assessment of TBCs is done by observing engine-tested components. On a simplistic level, impact damage can be considered as contact between a sphere (the particle) and a surface (Ref 16). Assuming that the particle momentum is wholly converted to normal force, contact normal and shear stresses introduced in the TBC are sufficient to cause spalling.

3. Spalling Life Modeling Approach

It is assumed that TBC spalling follows the weakest link theory (i.e., spalling occurs when the imposed stress exceeds the material strength) regardless of the TBC structure. Spalling occurs as a result of either monotonic (an overload/thermal rupture situation) or cyclic thermal loads. The typical failure mode is ceramic buckling due to compressive in-plane stresses at locations where the ceramic has become sufficiently disbonded by a near-interface crack. The life models focus on the material layer in which failure occurs. Specifically, the stress and strain at the TBC failure location are analytically determined and used to correlate TBC spalling life. Empirical TBC spalling life models are developed based on a combination of failure observations, TBC spalling life data, and stress analyses.

4. Life Modeling

4.1 *Plasma-Sprayed TBC*

Life modeling of plasma-sprayed TBC was based on a combination of metal oxidation and ceramic cyclic inelasticity (Ref 6). The life model followed a power-law relationship:

$$N_f = \Delta\varepsilon_f^{-b} \qquad \text{(Eq 5)}$$

$$\Delta\varepsilon_f = \left[\left(\frac{\Delta\varepsilon_{fo}}{\Delta\varepsilon_{in}}\right)\left(1-\frac{\delta}{\delta_c}\right)^c + \left(\frac{\delta}{\delta_c}\right)^c\right] \qquad \text{(Eq 6)}$$

A correlation of burner rig data from Ref 6 is presented in Fig. 8. The burner rig data consist of three generic test cycles: strain emphasis, oxide emphasis, and mixed mode. The strain emphasis cycle consists of a 2 min heating to maximum temperature and a 4 min cooling to about 38 °C (100 °F). The oxide emphasis cycle consists of a 1.5 min heating from about 538 °C (1000 °F) to maximum temperature, a several-minute dwell at maximum temperature, and then a 0.5 min cooling back to 538 °C (1000 °F). Finally, the mixed-mode cycle is a combination of strain emphasis heating and cooling transients and oxide emphasis dwell at maximum temperature. A modified Walker unified viscoplastic constitutive model was used to determine the ceramic inelastic strain range in the Ref 6 program. The observed TBC spalling life data from cyclic burner rig tests were correlated

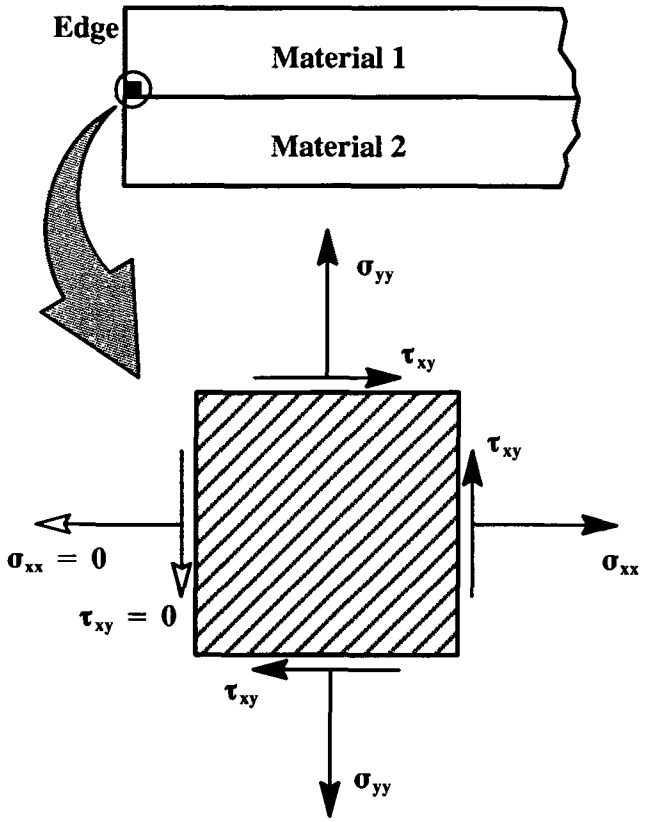

Fig. 6 Edge condition at the interface between two dissimilar materials

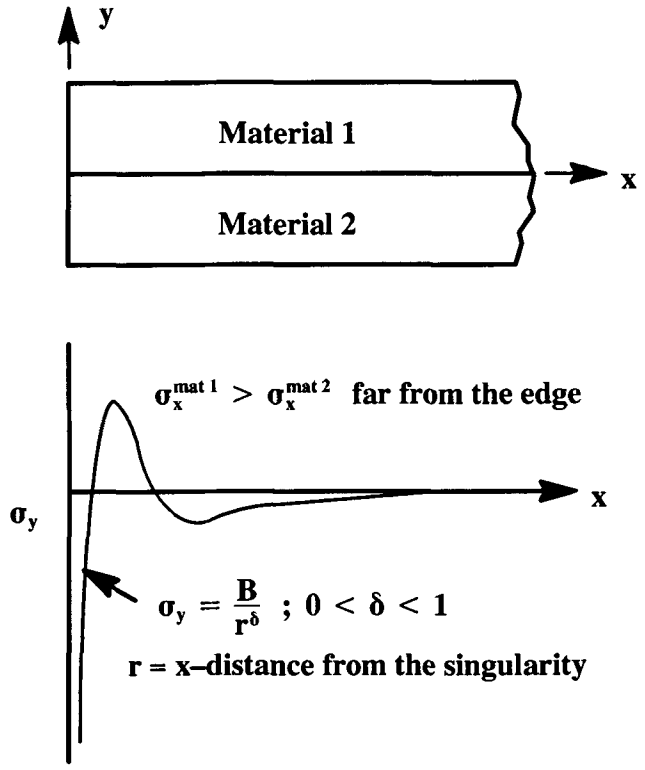

Fig. 7 General shape of the normal stress singularity along the interface

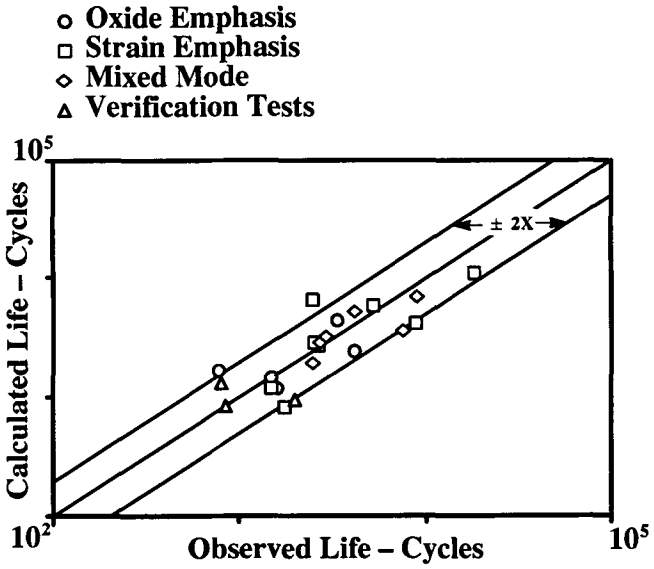

Fig. 9 EB-PVD TBC spalling life correlation. Source: Ref 7

within about a ±3× life scatter band, which is considered inadequate for TBC-coated component design application.

Of all the failure mechanisms, the stress introduced by interface roughness is considered the dominant mechanism that controls plasma-sprayed TBC delamination crack initiation. Detailed micrographic data (Ref 6) show that delamination cracks initiate at (or very near) the peaks of the rough interface,

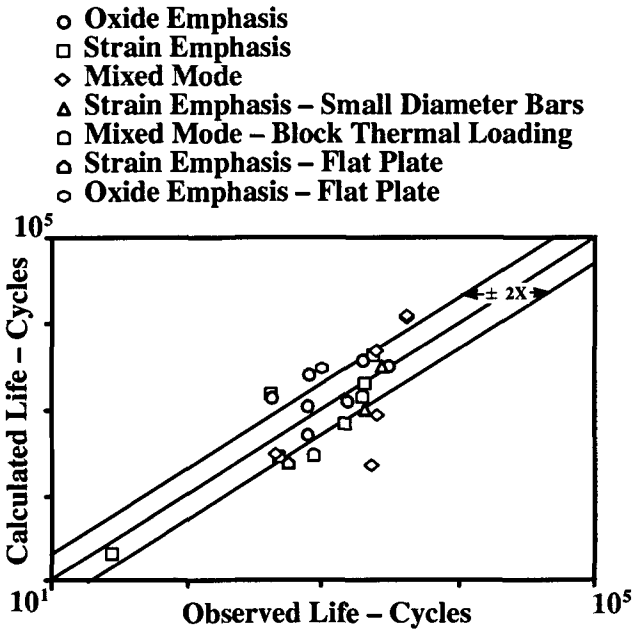

Fig. 8 Plasma-sprayed TBC spalling life correlation. Source: Ref 6

where the tensile stress normal to the interface is highest. Even in the absence of significant TGO buildup and thermal gradients (specimen furnace exposure in argon), TBC delamination cracks were observed emanating adjacent to the bond coat peaks (Ref 6). Also, flat plate and small-diameter rig specimen data indicate that the rough interface overwhelms any radius of curvature effect (Ref 6). Initial investigation of a wavy interface stress field is provided in Ref 4 and 9. In general, however, the stress field along the rough interface may change dramatically as the interface morphology evolves by diffusion processes (e.g., ceramic sintering and TGO formation). Understanding the effects of such processes is necessary prior to making TBC life model modifications.

4.2 *EB-PVD TBC*

Life modeling of EB-PVD TBC was based on a combination of metal oxidation (TGO formation) and TGO tensile strain (Ref 7, 8). The life model followed the power-law relationship of Eq 5 and 6. A correlation of burner rig data from the Ref 7 program is presented in Fig. 9. The correlation capability is within about a ±2× life scatter band, which is considered acceptable for TBC-coated component design purposes.

However, the notion that the TGO is in tension is suspect. A review of the TGO displacement calculation in the Ref 7 program indicates that the calculated TGO tensile strain is erroneous. As mentioned previously, TGO formation is a volumetric expansion process that is constrained by the stiffness of the substrate. As a result, the TGO is initially in in-plane compression, which is contrary to the Ref 7 model. Cooling to ambient conditions increases the TGO compression due to thermal expansion mismatch strains. Thus, the TGO in-plane strain should be entirely compressive.

Based on the preceding argument and a review of EB-PVD ceramic microstructures and spalling data from the Ref 7 pro-

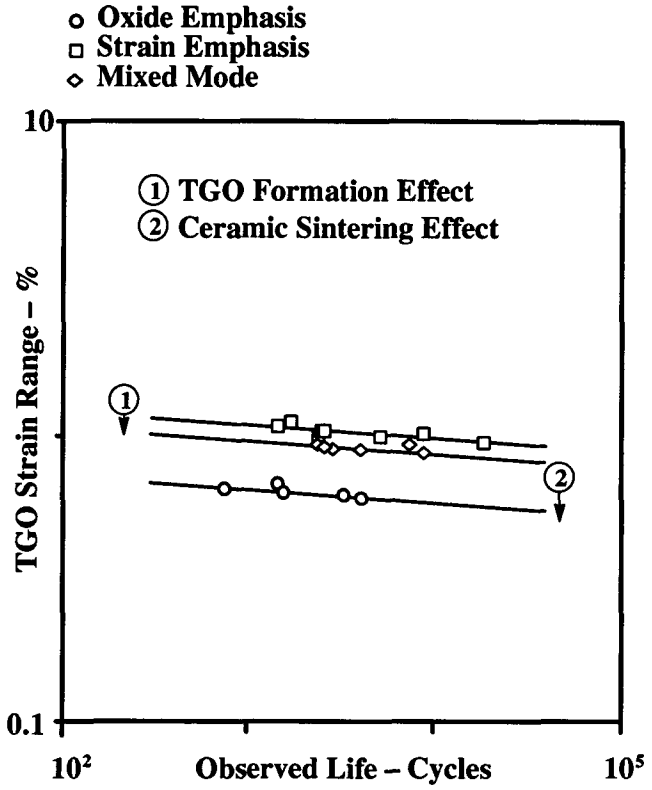

Fig. 10 EB-PVD TBC spalling life correlation using TGO strain range

gram, the following conceptual EB-PVD TBC spalling life prediction model is proposed. Since the TGO is in compression regardless of the cycle type, the TGO mechanical strain range is used as a starting point. Thermally grown oxide strain range versus life for the Ref 7 data is presented in Fig. 10. Notice that TGO strain range and thickness (dependent on thermal exposure time) qualitatively correlate the strain emphasis and mixed-mode tests (i.e., the mixed-mode cycle equals the strain emphasis cycle plus dwell at maximum temperature). However, for equivalent TGO thicknesses, the oxide emphasis tests spalled much sooner than the mixed-mode tests. The shorter oxide emphasis lives can be explained by including the effects of EB-PVD ceramic structure sintering. Ceramic microstructures of the strain emphasis and mixed-mode tests are similar. Cycling to near-room temperature tended to break any bonds between ceramic columns caused by sintering. The oxide emphasis cycle minimum temperature was about 538 °C (1000 °F). Sintering bonds were left relatively intact in the oxide emphasis cycle (Ref 7). Thus, the ceramic columnar structure is somewhat destroyed and the residual compressive stress is greater (which makes TBC failure more likely) than either of the other two cycle types. The apparent effect of sintering on ceramic behavior is shown in Fig. 11.

5. Conclusions

Further experimental and analytical investigation of plasma-sprayed and EB-PVD TBC is needed to characterize TBC de-

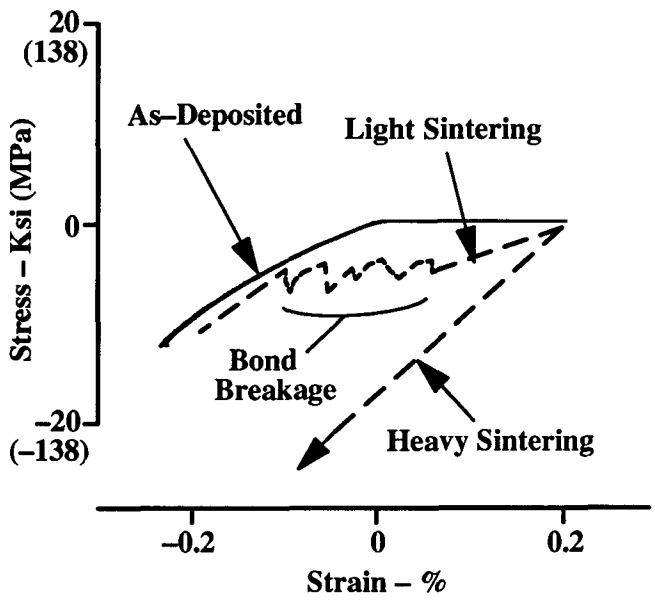

Fig. 11 Effects of sintering on EB-PVD ceramic in-plane stress

lamination crack initiation and growth mechanisms that lead to TBC spalling. Available rig data indicate that TBC spalling typically occurs as a result of ceramic layer buckling at locations where the ceramic has disbonded from the metal. Existing TBC spalling life models (Ref 6-8) are inconsistent with the TBC buckling failure mode. Development of an accurate plasma-sprayed TBC spalling life model requires a more thorough understanding of the rough interface stress field.

An improved EB-PVD spalling life model is suggested based on a combination of TGO formation and ceramic sintering. The proposed EB-PVD model qualitatively captures the observed spalling life trends and is consistent with the TBC buckling failure mode.

References

1. B.L. Koff, "Spanning the Globe with Jet Propulsion," Paper 2987, presented at AIAA 1991 Annual Meeting and Exhibit (Arlington, VA), American Institute of Aeronautics and Astronautics, 30 April-2 May 1991
2. K.D. Sheffler and D K. Gupta, Current Status and Future Trends in Turbine Application of Thermal Barrier Coatings, *J. Eng. Gas Turbines Power (Trans. ASME)*, Vol 110, 1988, p 605-609
3. P.A. Siemens and W.B. Hillig, "Thermal-Barrier-Coated Turbine Blade Study," NASA CR-165351, NASA–Lewis Research Center, Aug 1981
4. A.G. Evans, G.B. Crumley, and R.E. Demaray, On the Mechanical Behavior of Brittle Coatings and Layers, *Oxid. Met.*, Vol 20 (No. 5-6), 1983, p 193-216
5. C.A. Andersson, Thermal Stress Fracture of Ceramic Coatings, *Fract. Mech. Ceram.*, Vol 6, 1983, p 497-509
6. J.T. DeMasci, K.D. Sheffler, and M. Ortiz, "Thermal Barrier Coating Life Prediction Model Development, Phase I—Final Report," NASA CR-182230, NASA–Lewis Research Center, Dec 1989
7. S.M. Meier, D.M. Nissley, and K.D. Sheffler, "Thermal Barrier Coating Life Prediction Model Development, Phase II—Final Report," NASA CR-189111, NASA–Lewis Research Center, July 1991

8. S.M. Meier, D.M. Nissley, K.D. Sheffler, and T.A. Cruse, Thermal Barrier Coating Life Prediction Model Development, *J. Eng. Gas Turbines Power (Trans. ASME)*, Vol 114, 1992, p 258-263

9. G.C. Chang, W. Phucharoen, and R.A. Miller, "Thermal Expansion Mismatch and Plasticity in Thermal Barrier Coating," NASA CP-2493, NASA–Lewis Research Center, Oct 1987, p 357-368

10. D.M. Nissley, "Layer User and Programmer Manual," NASA CR-187038, NASA–Lewis Research Center, Oct 1990

11. D.M. Nissley, T.G. Meyer, and K.P. Walker, "Life Prediction and Constitutive Models for Engine Hot Section Anisotropic Materials Program—Final Report," NASA CR-189223, NASA–Lewis Research Center, Sept 1992

12. K.S. Chan, U.S. Lindholm, and S.R. Bodner, "Constitutive Modeling for Isotropic Materials (HOST)—Final Report," NASA CR-182132, NASA–Lewis Research Center, June 1988

13. A.D. Freed and K.P. Walker, "Refinements in a Viscoplastic Model," NASA TM-102338, NASA–Lewis Research Center, Dec 1989

14. A.-Y. Kuo, Thermal Stresses at the Edge of a Bimetallic Thermostat, *J. Appl. Mech.*, Vol 56, 1989, p 585-589

15. M. Bak and H.A. Koenig, Prediction of Edge Stresses in Layered Media Using the Surface Integral-Finite Element Technique, *Eng. Fract. Mech.*, Vol 48 (No. 4), 1994, p 583-593

16. R.J. Roark and W.C. Young, *Formulas for Stress and Strain*, 5th ed., McGraw-Hill, 1982, p 516